Magnetic Properties of Manganese Ferrite Nanoparticles

A Thesis submitted

In Partial Fulfillment of the Requirements

for the degree of

MASTER OF TECHNOLOGY

in

MATERIALS & METALLURGICAL ENGINEERING

BY

ROWAID RAAD MUSLIM
(ROLL NO. 601002008)

SCHOOL OF PHYSICS AND MATERIALS SCIENCE
THAPAR UNIVERSITY
PATIALA-147004
INDIA
June 2012

CERTIFICATE

This is to certify that the thesis entitled "Magnetic Properties of Manganese Ferrite Nanoparticles" submitted by Mr. Rowaid Raad Muslim is in partial fulfillment for the degree of Master of Technology in Materials & Metallurgical Engineering embodies the work carried out by Mr. Rowaid Raad Muslim under my supervision in the School of Physics and Materials Science, Thapar University, Patiala. He has not submitted this work to any other University or Institute for the award of any degree.

Dr. S. D. Tiwari
Assistant Professor
School of Physics and Materials Science
Thapar University, Patiala

Countersigned by

Dr. Kulvir Singh
Head
School of Physics & Materials Science
Thapar University, Patiala

Dr. S. K. Mohapatra
Dean of Academic Affairs
Thapar University, Patiala

DECLARATION

I hereby declare that the thesis entitled "Magnetic Properties of Manganese Ferrite Nanoparticles" is the work carried out by me under the supervision of Dr. S. D. Tiwari. I have not submitted this work anywhere else for the award of any degree.

Rowaid Raad Muslim

ACKNOWLEDGEMENT

First, my thanks and praise to Allah, the God of the worlds for all the blessings for me and my family.

I express my thanks to my thesis supervisor Dr. S. D. Tiwari for his keen interest, valuable guidance, strong motivation and constant encouragement during the course of the work.

I would like to thank Dr. Kulvir Singh (Head, School of Physics and Materials Science), Dr. O. P. Pandey, Dr. Puneet Sharma and Dr. Bhupendra Kumar Chudasama for their constant guidance and encouragement.

Special thanks to my parents, my brother and my sisters for their support and encouragement.

Finally, I would like to thank all my classmates and friends I did meet in India for their friendship.

Rowaid Raad Muslim

ABSTRACT

$MnFe_2O_4$ nanoparticles having average crystallite sizes of about 7 and 9 nm are synthesized using co-precipitation method. Samples are characterized by X-ray diffraction, transmission electron microscope and vibrating sample magnetometer. Magnetic properties of both the samples are studied and compared.

CONTENTS

LIST OF FIGURES

Chapter 1
Introduction

1.1 Introduction

Magnetic nanomaterials have become important area of research because of their interesting properties and useful applications. Nanoparticles of magnetic materials are useful for variety of applications such as data storage, magnetic fluid, magnetic resonance, biotechnology etc. However for successful applications these nanoparticle systems must be highly under different conditions. Nanoparticles of magnetic materials start showing interesting behaviors when the size of the particles is below a critical size. This critical size is material dependent but is typically few tens of nanometer.

The method for preparation of magnetic nanoparticles is very important because it controls the size distribution, shape, morphology etc. of the particles on which its behaviors strongly depend. Manganese ferrite is a soft ferrite [1]. It has high magnetic permeability and low losses. This material is very useful in many areas of engineering such as computer memory chip, microwave devices, magnetic recording media, transformer coil, magnetic recording media etc. Because of these important applications this material is very popular among scientists and engineers for research. Many people are still working on this material because of possibility for its potential applications in different devices.

1.2 Magnetic Behavior

The materials around us consist of atoms and the atom consists of positively charges nucleus surrounded by negatively charged electrons clouds. The nucleus of atom consists positively charged protons and neutral neutrons. In an atom the electron has two types of motions i.e. orbital motion and spin about its own axis. These two types of motions of the electron in the atom produce a magnetic moment. The direction of magnetic moment is determined by the directions of spin and orbital motion of the electron. In other words the atom possesses magnetic moment in two ways. The first is due to orbital motion of electron and the second is due to its spin around its own axis. The total magnetic moment is the vector sum of orbital magnetic moment and spin magnetic moment [2].

In any material the relative arrangements of atomic spins decide its behavior in external applied magnetic field. Based on the behaviors of materials in external applied magnetic all the materials can be classified into following main categories [1-4].

1.2.1 Diamagnetic Materials

The diamagnetic materials are repelled by a magnet. In presence of non uniform magnetic field the diamagnetic materials move from stronger to weaker part of the magnetic field. The susceptibility of diamagnetic material is negative. Examples of diamagnetic materials are Copper, Diamond, Antimony, Bismuth, Gold, Mercury, Silver, Tin, Zinc etc.

In the presence of external applied magnetic field the magnetization of the diamagnetic material is opposite to the applied field. If the external applied magnetic field is removed then the magnetization of the material becomes zero.

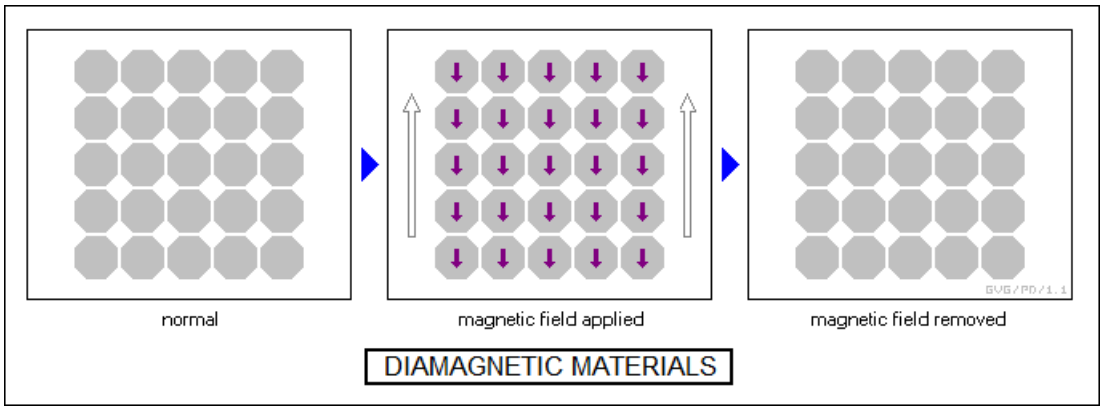

Figure 1.1: Diamagnetism. [5]

1.2.2 Paramagnetic Materials

The paramagnetic materials are weakly attracted by a magnet. If the paramagnetic material is placed in external magnetic field then it experiences a weak force. The direction of this force is towards to higher magnetic field. Examples of paramagnetic materials are Aluminum, Chromium, Copper sulphate, Manganese, Palladium, Platinum, Potassium and Tungsten etc.

In absence of external applied field the atomic moments are randomly oriented giving rise to zero magnetization. In the presence of external magnetic field the atomic moments try to align themselves along the field direction giving a positive magnetization.

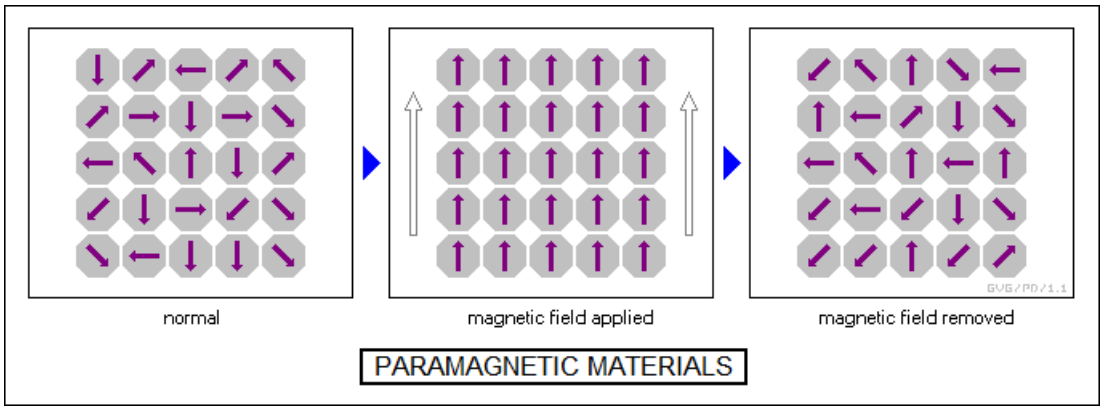

Figure 1.2: Paramagnetism. [5]

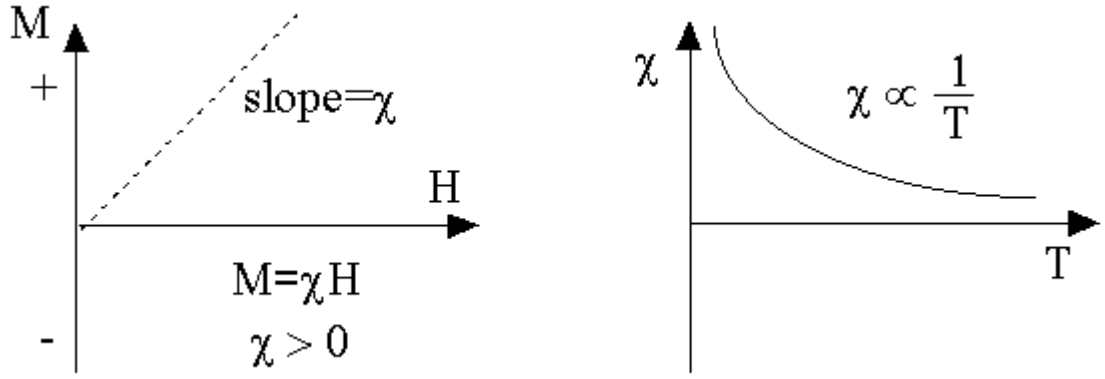

Figure 1.3: M vs. H and χ vs. T curves for paramagnetic material. [6]

In the presence of small magnetic field the magnetization of paramagnetic material increases with increasing magnetic field linearly. The magnetization of paramagnetic material follows the Curie law i.e. for paramagnetic material

$$M = C\,(H / T)$$

where C is the Curie constant. In other words the susceptibility of paramagnetic material varies as

$$\chi = C / T$$

1.2.3 Ferromagnetic Materials

Ferromagnetic materials are attracted by a magnet. These materials have very large values of magnetic permeability. Also they have very large degree of magnetization. Examples of ferromagnetic materials are Iron, Cobalt, Nickel etc.

In ferromagnetic materials the atomic magnetic moments are aligned parallel to each other. This is due to strong exchange interaction among atomic magnetic moments. This exchange interaction is very strong in nature but is short range. The dipolar interaction also acts among the atomic magnetic moments. This dipolar interaction is weak but is long range in nature. There use to be a competition between these two types of interaction among all the atomic magnetic moments inside any ferromagnetic material. The energy of the system can minimized if it divides itself in a very large number of regions called magnetic domains. In a particular domain all the atomic magnetic moments are aligned along same direction. However the boundary of any magnetic domain can not be sharp. Between two domains the atomic magnetic moments change their directions gradually over some distance. This region is known as Bloch wall. In this way the system can further minimize the energy. Usually all the domains are oriented randomly. This gives rise to zero magnetization. But the magnetization within each domain still remains non zero.

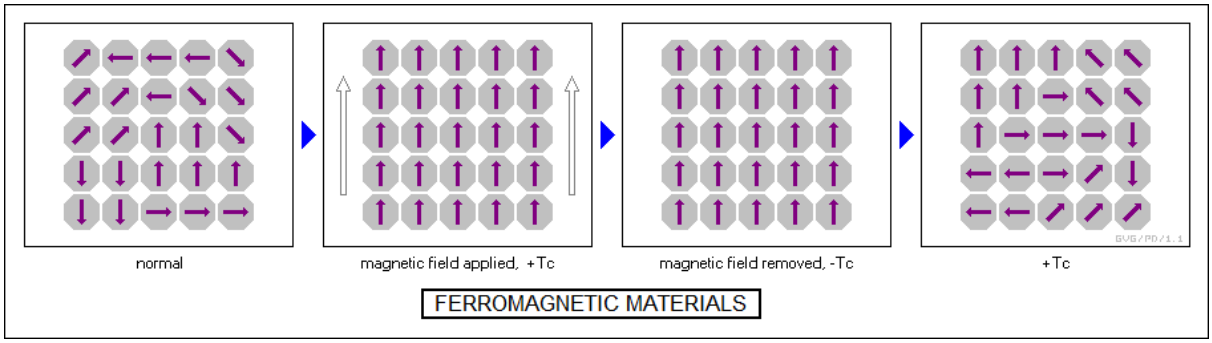

Figure 1.4: Ferromagnetism. [5]

A ferromagnetic material becomes paramagnetic at a critical temperature T_C, known as the Curie temperature. At this temperature the thermal energy is sufficiently large to overcome the strong exchange interaction energy among atomic magnetic moments. Because of this reason the ferromagnetic ordering inside the material is disturbed and the material becomes paramagnetic. Above this Curie temperature the susceptibility of the material is expressed by relation

$$\chi = C / (T - T_C)$$

where C is a material dependent constant.

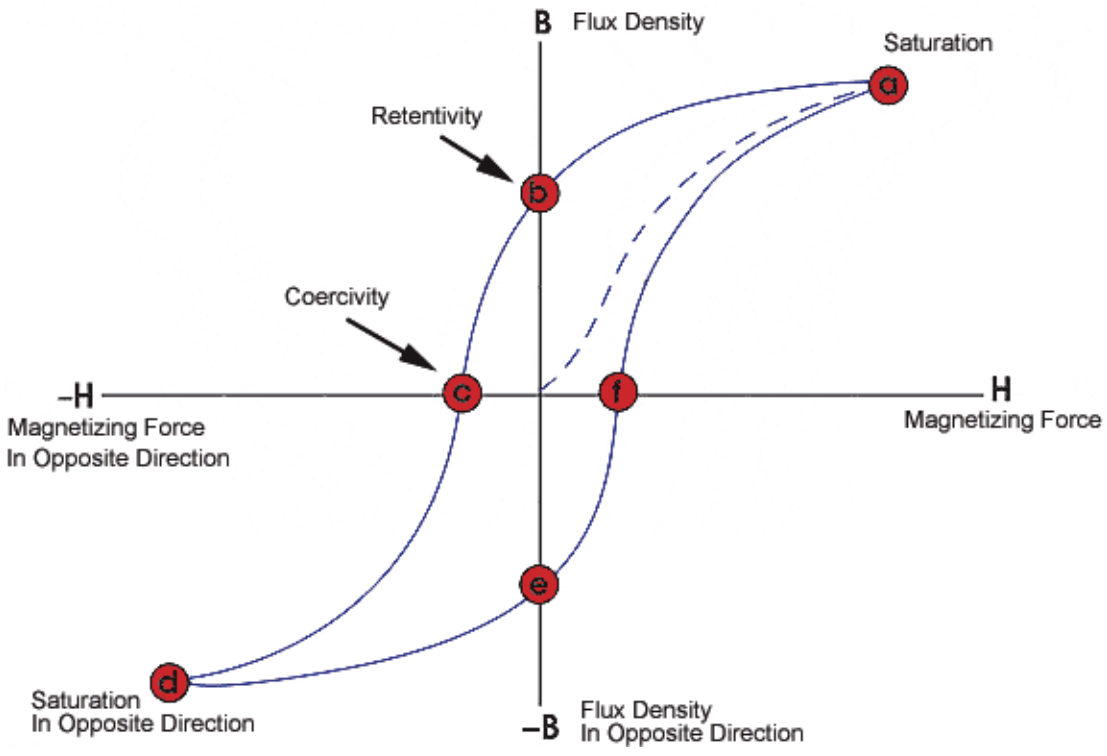

Figure 1.5: M vs. H loop for ferromagnetic material. [7]

Figure 1.5 shows magnetization versus applied magnetic field curve for a ferromagnetic material below the Curie temperature. The magnetic induction B increases with increasing strength of external applied magnetic field H. At point ‘a’ magnetic flux density B saturates. In other words if the magnetizing field is further increased then there will not be any increase in the magnetic flux. At this point all magnetic domains are aligned in same direction. Now if the magnetizing field decreases then the magnetic flux density B reaches to point ‘b’ from point ‘a’. At this point ‘b’ magnetizing field is zero but magnetic flux density remains non zero. This existing magnetic flux is called retentivity of the material. The magnetic flux density reaches to zero that is at point ‘c’ for further decrease in the applied magnetizing field. This negative applied magnetizing field at which the flux density becomes zero is known as coercivity of the material. At this point all the domain give rise to a net zero flux. Further increase in the magnetizing field in negative direction causes an increase in flux and become saturated at point ‘d’ in opposite direction. The curve reaches at point ‘e’ which is residual magnetism when magnetizing field is again reduced to zero. On further increasing the magnetizing field in positive direction the flux density again reaches to zero value at point ‘f’.

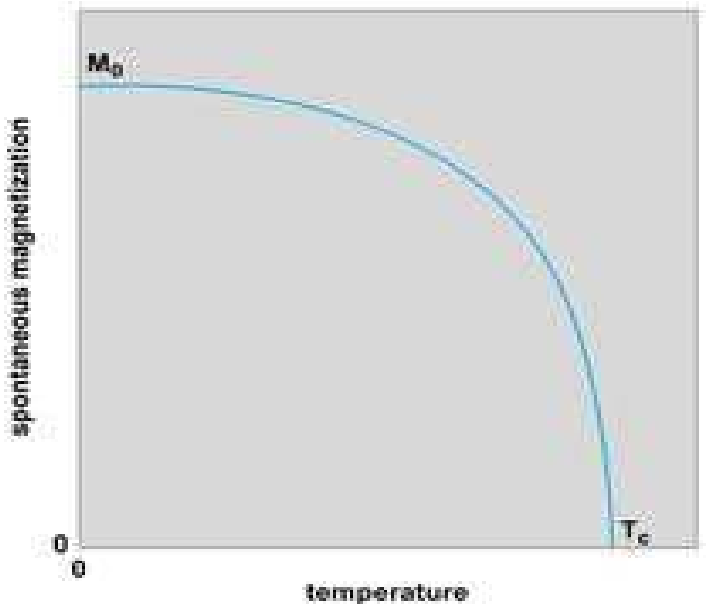

Figure 1.6: Magnetization as a function of temperature for ferroagnetic material. [8]

The magnetization of any ferromagnetic material remains unchanged in a constant applied magnetic field at constant temperature. The magnetization of the ferromagnetic material decreases with increasing temperature. The magnetization of the system becomes zero at Curie temperature T_C as shown in Figure 1.6.

1.2.4 Antiferromagnetic Materials

In antiferromagnetic materials the atomic spins are aligned antiparallel to each other as shown in Figure 1.7. The magnitude of all the spins are same. Because of this reason the antiferromagnetic material posses zero net magnetization. At a critical temperature, known as the Neel temperature T_N, this antiferromagnetic ordering breaks and the antiferromagnetic material becomes paramagnetic. Well above this temperature the susceptibility of the material is described by relation

$$\chi = C / (T + T_N)$$

where C is a material dependent constant.

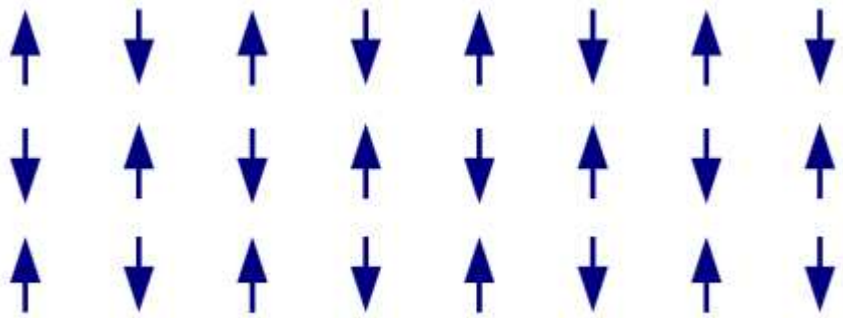

Figure 1.7: Arrangement of spins in antiferromagnetic materials. [9]

The antiferromagnetic material can be considered to consists of two sub lattices. The magnetization of one sublattice is equal and opposite to the other. Due to this the net dipole moment or magnetization of antiferromagnetic material is zero in the absence of external magnetic field. If the material is placed in external magnetic field a small magnetization in the direction of the field is produced. This magnetization increases with increasing temperature and becomes maximum at Neel temperature. The magnetization starts decreasing for any further increase in the temperature.

1.2.5 Ferrimagnetic Materials

Ferrimagnetic ordering is a special case of antiferromagnetic ordering. In this ordering the magnetization of one sublattice is different from that of the second lattice. This situation results in a non-zero magnetization for the system. At a critical temperature the ferrimagnetic ordering breaks and the material becomes paramagnetic.

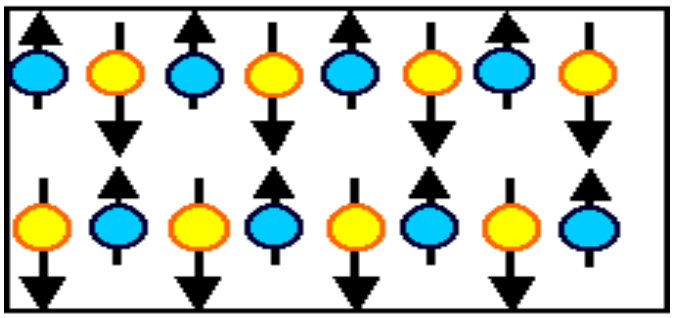

Figure 1.8: Ferrimagnetic ordering. [10]

A well known example of ferromagnetic material is magnetite (Fe_3O_4). This is also known as lodestone. This oxide has an inverted spinel structure generally described as an FCC lattice of O^{2-} ions that form cages surrounding interstitial sites. Spinels are also viewed as having an admixture of rocksalt and zinc blende packing. Figures 1.9 and 1.10 illustrate the structure of normal and inverted spinel structure of ferrites. In the indicated cubic cell, one-eighth the size of the normal unit cell, there are eight tetrahedral sites. One of these is occupied by a Fe^{3+} ion with a spin pointing downward. Two of four octahedral sites in the cell are also occupied, one by an Fe^{3+} ion and one by an Fe^{2+} ion, both with upward spin. Thus, the compound can be written as $Fe^{2+}Fe_2^{3+}O_4$ in this octant cell, or $(Fe^{2+}Fe_2^{3+}O_4)_8$ in the normal cell. Other magnetic ferrites have inverted spinel structures in which the magnetic moment may be viewed as deriving solely from the divalent cation. The Fe^{3+} ions on tetrahedral and octahedral sites couple anti-ferromagnetically, resulting in a cancellation of the moment from this source. A rich variety of ferrite alloys having the general formula $Me^{2+}Fe_2^{3+}O_4$, where Me^{2+} is a divalent metal ion that substitutes for Fe^{2+} (e.g., Ni^{2+}, Co^{2+}, Zn^{2+}), is possible [1]. For example, in $Co^{2+}Fe_2^{3+}O_4$, a mole of CoO is alloyed with one of Fe_2O_3. The subunit cell magnetization depends only

on the Co^{2+} ion moment of $3\mu_B$. Because of moment cancellation in adjacent sublattices, the saturation magnetization of ferrites is generally less than that of metal magnets.

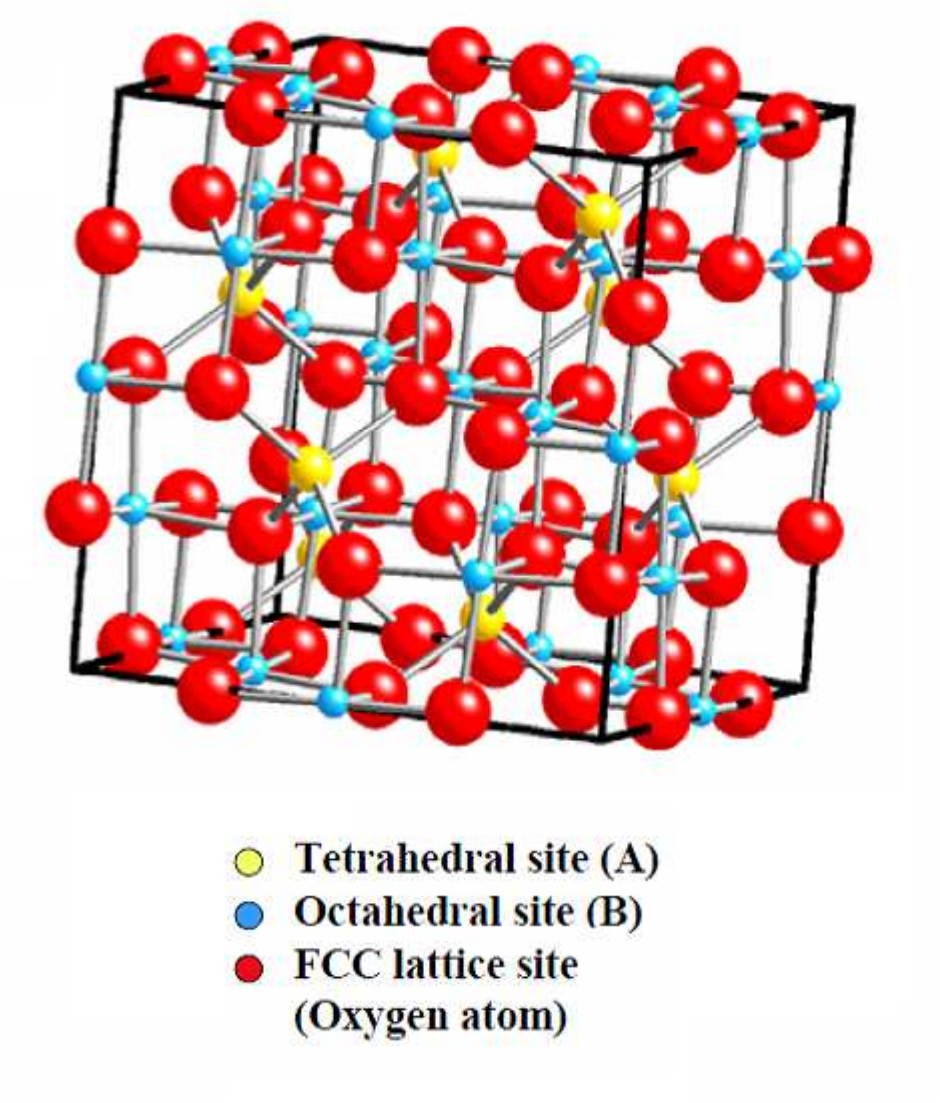

Figure 1.9: Normal spinal structure. [11]

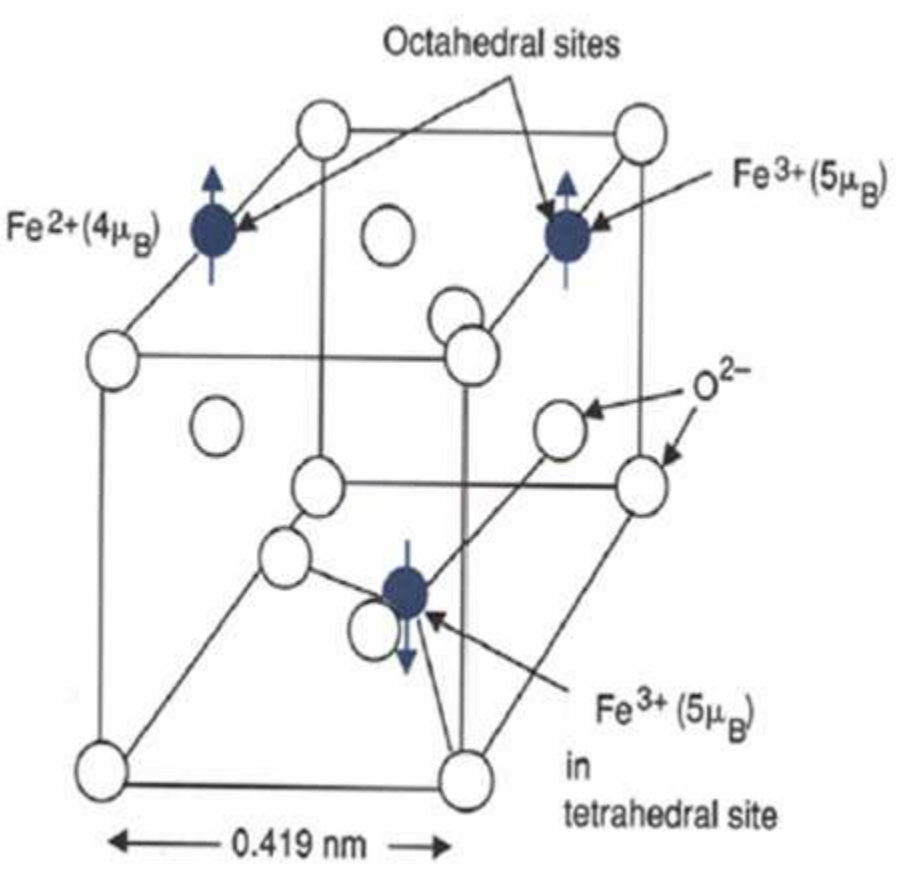

Figure 1.10: The inverse spinal structure of ferrite of the type $MeFe_2O_4$, emphasizing the magnetization of ions in octahedral and tetrahedral sites within one octant of the normal unit cell. [12]

1.3 Magnetic Anisotropy

Anisotropy is existence of properties which depend on the direction. Magnetic anisotropy is an important characteristic of any magnetic material. This is important from fundamental point of view as well as for technological applications. Depending on the requirement magnetic material having low or high magnetic anisotropy may be required. Due to this a good understanding of origin of magnetic anisotropy is required.

1.3.1 Magnetocrystalline Anisotropy

There are certain preferred directions along which the magnetization vector of any magnetic material can be easily oriented. This direction is known as easy axis. There are also directions along which it is most difficult to align the magnetization vector. This direction is known as hard axis.

Cobalt has hexagonal structure and is ferromagnetic in nature. The hexagonal c-axis is the easy axis for cobalt. It means that it is easiest to orient the magnetization vector along the c-axis (or opposite to the c-axis). Such type of situation is known as unidirectional magnetocrystalline anisotropy. If θ is the angle between magnetization vector and the easy axis then the magnetocrystalline anisotropy energy is given by

$$E_{an} \approx K V \mathrm{Sin}^2 \theta$$

where V is the volume of the crystal and K is anisotropy constant. From this relation it is clear that the system has equal energy for $\theta = 0^0$ or 180^0. However it requires energy K V to flip the magnetization vector from $\theta = 0^0$ to 180^0. From this relation it is also clear that

the magnetocrystalline anisotropy energy is directly proportional to the volume of the crystal.

Figure 1.11 shows magnetization curves along with the directions of easy and hard axis for magnetite. The magnetization reaches saturation in presence of different applied magnetic field depending on the crystallographic orientation of the sample in the external applied magnetic field. From this figure it is clear that <111> is the easy direction of magnetization and <100> is the hard direction of magnetization for magnetite. Also <110> is the intermediate direction of magnetization.

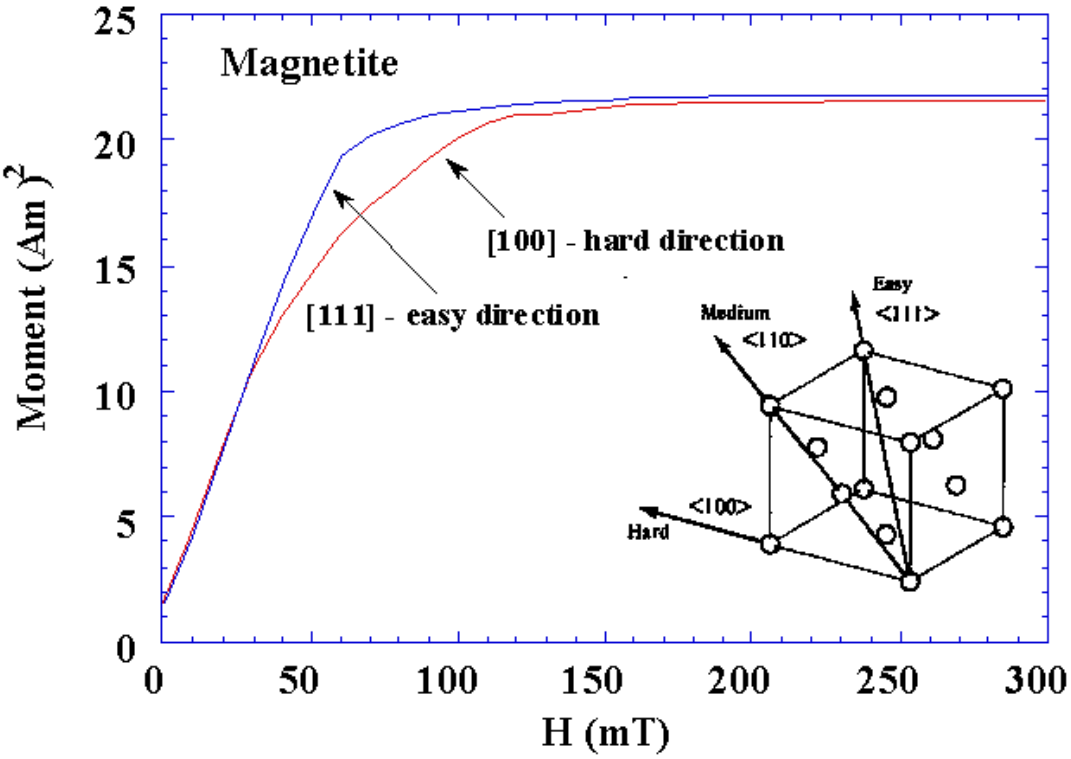

Figure 1.11: Directions for easy and hard magnetizations for magnetite. [13]

1.3.2 Stress Anisotropy

The exchange interaction energy depends on interaction between orbitals of neighboring atoms inside the material. If the position of an atom inside the material changes then the exchange interaction is affected. Therefore if positions of atoms inside any material are change by the applications of a strain then the magnetic behavior of the material will be changed. If a ferromagnetic material is placed in a magnetic field then the crystal experiences a strain. This strain is a function of applied magnetic field. This strain changes the dimensions of the material. This phenomenon is called magnetostriction. For example if iron crystal is placed in a magnetic field directed along the easy direction [100] then it gets longer along this direction but contracts in transverse directions [010] and [001]. The quantity δl/l is called magnetostrictive constant λ.

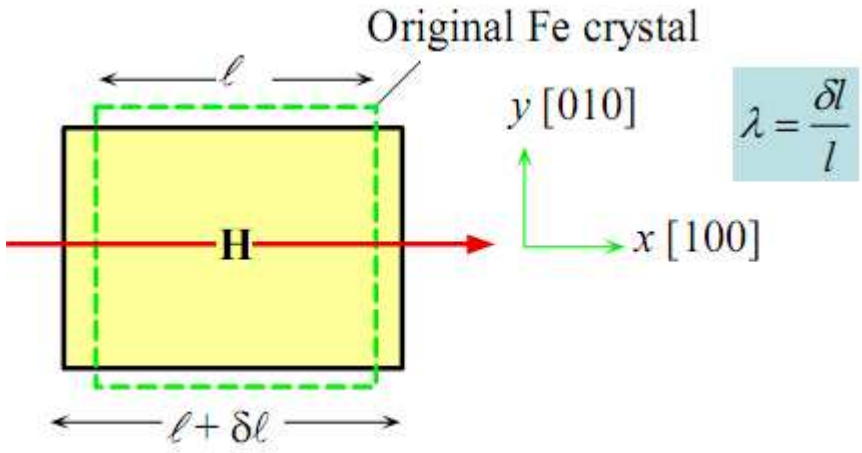

Figure 1.12: Change in the dimensions of a sample by the application of magnetic field. [14]

1.3.3 Shape Anisotropy

The type of anisotropy that arises due to the shape of a crystal is known as shape anisotropy. If a sample is magnetized by the application of external magnetic field H_e then it produces magnetic charges on its surface. This polarity generates new magnetic field along a direction opposite to the applied magnetic field. This induced field is called demagnetizing field. The value of the demagnetizing field changes with the change in the direction of the external applied magnetic field. The shape anisotropy is demonstrated in Figure 1.13.

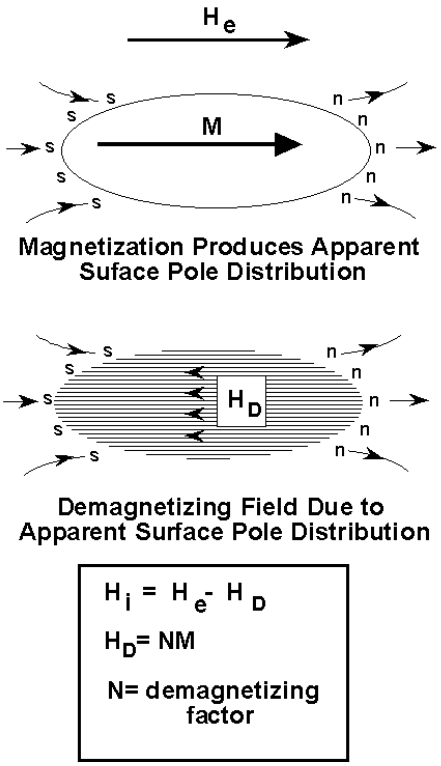

Figure 1.13: Shape anisotropy. [15]

1.4 Superparamagnetism

The magnetization vector of any ferro or ferromagnetic crystal will be aligned along the easy axis to minimize the magnetocrystalline anisotropy energy under normal conditions. In earlier discussion it has been mentioned that the magnetocrystalline anisotropy energy of any crystal is directly proportional to the volume of the crystal. If volume of any crystal is sufficiently reduced such the thermal energy becomes larger than the magnetocrystalline anisotropy energy then the magnetization vector of the crystal will be no longer fixed and will flip. This situation becomes similar to paramagnetism and known as superparamagnetism. The paramagnetism is shown by paramagnetic ions inside solid having magnetic moments of few Bohr magnetons. The superparamagnetism is shown by small particles of magnetic materials having magnetic moment of few thousand Bohr magnetons.

Figure 1.14 (a) shows plot of magnetization as a function of magnetic field for iron nanoparticles at different temperatures. Figure 1.14 (b) shows plot of magnetization as a function of (H/T) for iron nanoparticles. It is clearly seen that all the data points are almost lying on a single curve. In other words the magnetization of ferromagnetic nanoparticles is only function of (H/T). This is one of the characteristics of superparamagnetic particles.

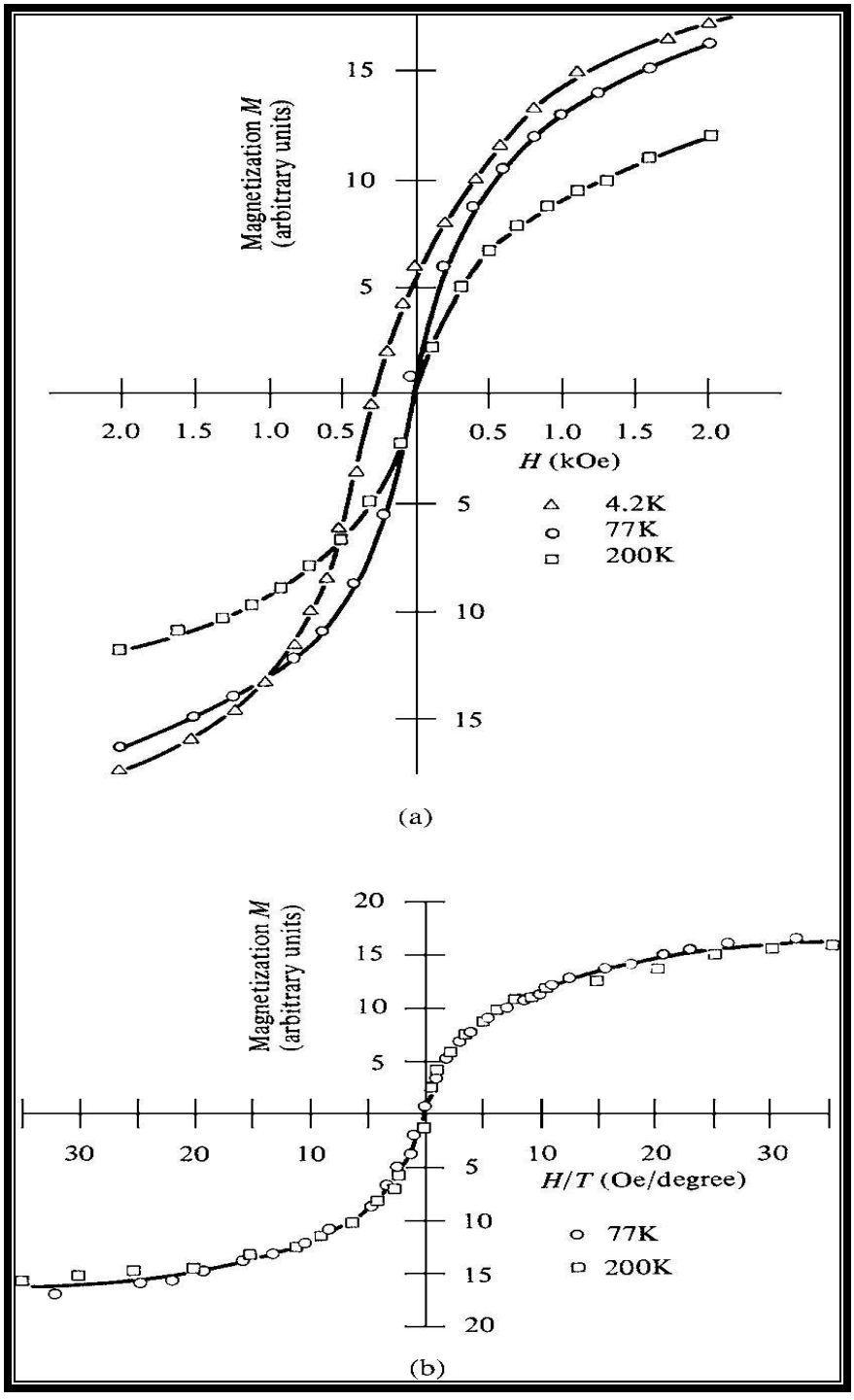

Figure 1.14: (a) M vs. H curves for iron nanoparticles. (b) Plot of M vs. (H/T) for iron nanoparticles. [16]

1.5 Literature Review and Aim of the Thesis

Different types of ferrites having different compositions have been studied and used for a long in useful applications. Research on different ferrites is vast and it is difficult to present all the findings. Therefore I present a brief review of the field as below.

Susan et al. [17] synthesized $MnFe_2O_4$ using co-precipitation and combustion techniques. Data show that the sample shwn better particulate properties with more nano sized particles when compared with samples prepared with other methods. N. S. Gajbhiye et al. [18] synthesized $MnFe_2O_4$ nanostructured particles by the citrate precursor method. The mechanism of thermal decomposition is examined in details. Nanocrystalline manganese ferrite particles having crystallite size of 7.0 nm were formed at 350 $^{\circ}$C. Amighian et al. [19] synthesized manganese ferrite using co-precipitation method using aqueous solutions of $FeSO_4.7H_2O$, $MnSO_4.H_2O$ and NaOH. M. A. Ahmed et al. [20] prepared manganese ferrite by five different methods. These methods are flash combustion, co-precipitation, sol–gel, citrate precursor and the standard ceramic technique. All the samples were compared. T. V. Solis et al. [21] synthesized manganese ferrite by nanocasting technique. A low cost mesoporous silica gel as hard template was also used. Deraz and Shaban [22] synthesized single domain manganese ferrite nanoparticles with narrow particle size distribution using combustion technique. Effects of fuel ratios on the prepared powder samples were characterized. Aria Yang et al. [23] synthesized manganese ferrite $MnFe_2O_4$ using a modified co-precipitation technique. For this metal chloride solutions were added to different concentrations of boiling NaOH solutions to control particle growth rate.

In this work nanoparticles of manganese ferrite are synthesized by coprecipetation method [24]. For the synthesis of manganese ferrite nanoparticles by coprecipetation method it is very important to maintain the stoichiometry of Mn^{2+} and Fe^{3+} ions in the solution. In the starting solution the ratio of Mn^{2+} and Fe^{3+} ions should be 1 : 2. Any imbalance in this will cause the formation of either $Mn(OH)_2$ or $Fe(OH)_3$ along with the manganese ferrite nanoparticles. Salts of Mn^{2+} and Fe^{3+} absorb water from atmosphere. Due to this it is difficult to ensure the required stoichiometry of ions in the solution. In this work formation of either $Mn(OH)_2$ or $Fe(OH)_3$ will be avoided to synthesize manganese ferrite nanoparticles [25]. Two samples of manganese ferrite nanoparticles will be synthesized and their magnetic properties will be compared.

Chapter 2

Experimental Techniques

2.1 X-ray Deffractometer

X-rays are electromagnetic radiation discovered by Rontgen in 1895. In electromagnetic spectrum these rays occupy the region between gamma rays and ultraviolet rays. X-ray photons are highly energetic having energy in range of 100 eV to 100 keV. X-ray diffraction is a very useful and non-destructive technique that provides detailed information about the crystal structure of a crystalline material.

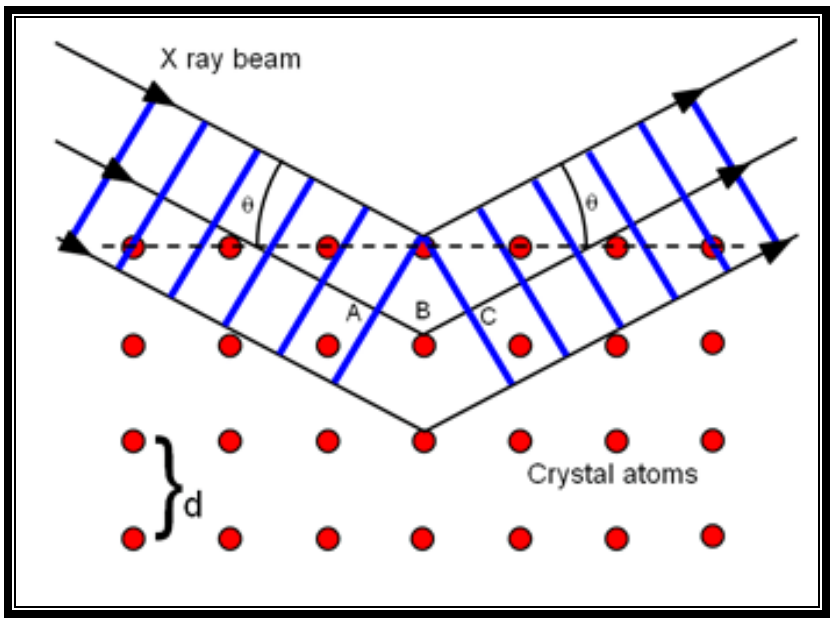

Figure 2.1: Bragg's reflection from atomic planes. [26]

Figure 2.1 illustrate Bragg's reflection of X-ray beam from a set of atomic planes in a crystal. The diffracted beam will of maximum intensity if

$$2 d \sin \theta = n \lambda$$

where λ is the wavelength of X-ray and n = 1, 2, ……. This is known as Bragg's law [1]. In X-ray diffraction intensity of diffracted beam is recorded as a function of angle 2θ. In this diffraction peaks are obtained at certain values of angle θ. Using Bragg's law the values of d are calculated and hence the material is characterized.

2.2 Transmission Electron Microscope

Microscope is an instrument that provides a magnified and resolved image of desired thing. Usually optical microscope is widely used for this purpose. Resolving power of any instrument depends on the wavelength of radiation used. This limits the resolving power of optical microscope.

In Transmission Electron Microscope an energetic beam of electrons is used. We can vary the wavelength of this beam by varying the energy of electrons in the beam. In this way a very high resolving power can be obtained. This microspore consist of magnetic lenses. Magnetic lenses are current carrying coils. With the help of these coils the beam of electrons can either be conversed or diverged. The image is formed on an imaging device such as a fluorescent screen, photographic film or CCD camera.

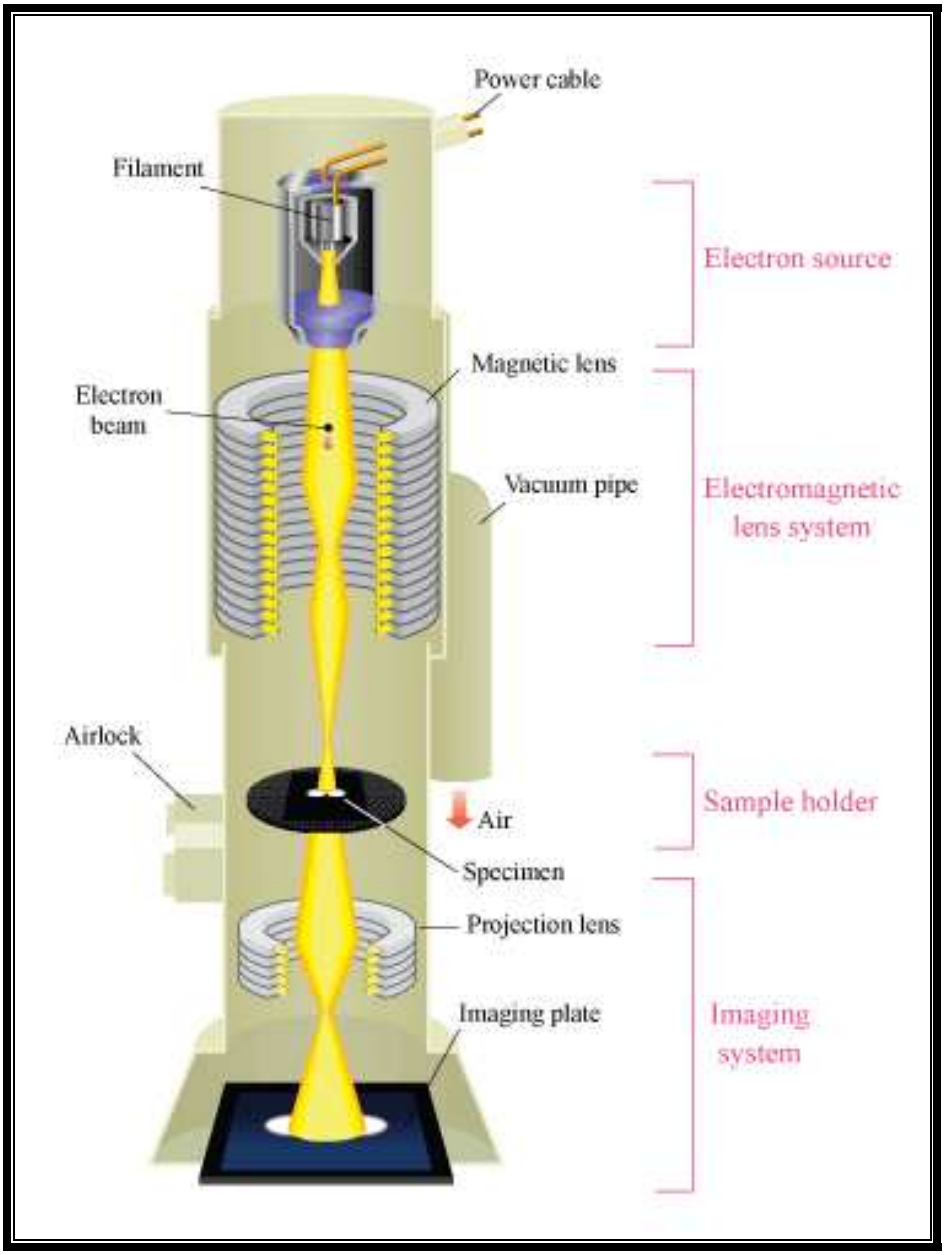

Figure 2.2: The schematic outline of a TEM. [27]

2.3 Vibrating Sample Magnetometer

A vibrating sample magnetometer is a scientific instrument that measures magnetization of a sample. It is based on Faraday's law of induction. In this instrument a magnetic is used to magnetize the sample. The magnetized sample is allow to vibrate vertically inside of pick up coil. An e. m. f. is induced across this coil. This induced e. m. f. is a measure of the magnetization of the sample and causes an electric current in the coil. This current is proportional to the magnetization of the sample. The higher is the magnetization, the larger is the induced current. The induction current is amplified by an amplifier. All the components are hooked up to a computer interface.

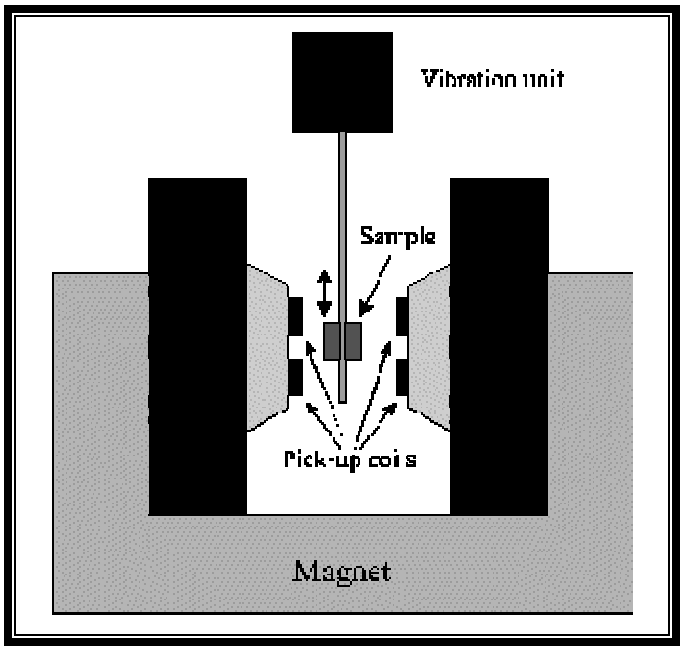

Figure 2.3: Schematic of a vibrating sample magnetometer. [28]

Chapter 3

Synthesis, Results & Discussion

3.1 Synthesis

In literature many physical and chemical methods are reported for the preparation of nanoparticles of any material. Chemical methods for the synthesis of nanoparticles are believed to be better than the physical methods because chemical reaction take place at molecular level. Because of this reason shape, size and morphology of the nanoparticles can be controlled in a better way. In this work I followed a chemical method for the synthesis of two different sizes $MnFe_2O_4$ nanoparticles. In this work the nanoparticles of $MnFe_2O_4$ are synthesized by a co-precipitation method [24, 25]. For this $Fe^{3+}$and Mn^{2+} ions in appropriate ratio in an aqueous solution are precipitated with the help of NaOH. Solution of NaOH is added drop wise in a solution containing Mn^{2+} and Fe^{3+} ions in stoichiometric amount. The resulting precipitate is of $MnFe_2O_4$. A very important step in this process is to maintain the ratio of Mn^{2+} and Fe^{3+} ions in the solution. In the starting solution the ratio of Mn^{2+} and Fe^{3+} ions should be 1 : 2. Any departure from this ratio will lead to formation of either $Mn(OH)_2$ or $Fe(OH)_3$. This formation of undesired product must be avoided by preparing solutions of Mn^{2+} and Fe^{3+} ions of known concentrations.

3.1.1 Preparation of $FeCl_3$ solution

Approximately 0.2 M solution of $FeCl_3.6H_2O$ is prepared by dissolving 0.2 mole $FeCl_3.6H_2O$ (i.e. 108.12g) in 1000 ml solution using a volumetric flask. From the volumetric flask, 50 ml solution is taken and diluted to 100 ml. This makes the concentration of this solution to be 0.1 M. From this diluted solution, 25 ml solution is taken in a conical flask. In this 20 ml concentrated HCl is added. The resulting solution is heated (at 70-90 ^{0}C) and reduced with $SnCl_2$ solution and then cooled. Because of this the Fe^{3+} ions present in the solution is converted into Fe^{2+} ions. Now the concentration of ferrous ions in the solution is estimated by titration method. For this 10 ml $HgCl_2$ solution is added and then diluted to about 250 ml. After this 15 ml concentrated H_2SO_4, 5 ml of phosphoric acid and 3 drops of diphenylamine indicator are added. The final solution is titrated with standard $K_2Cr_2O_7$ solution until colour changes from green to a pale blue (violet) colour. The whole process is repeated three times.

Reactions involving in this procedure are as follows

$$2Fe^{3+} + Sn^{2+} \rightarrow 2Fe^{2+} + Sn^{4+}$$

$$6Fe^{2+} + Cr_2O_7^{2-} + 14H^+ \rightarrow 6Fe^{3+} + 2Cr^{3+} + 7H_2O$$

3.1.2 Preparation of $MnCl_2$ solution

The amount of manganese in a solution of manganese chloride is decided by a gravimetric method. In this method, the manganese is precipitated as ammonium manganese phosphate ($MnNH_4PO_4.H_2O$) in slightly ammonical solution containing excess of ammonium salts. After drying at 100-105 ^{0}C the precipitate is ignited and weighted as $Mn_2P_2O_7$.

Approximately 0.2 M solution of $MnCl_2.2H_2O$ is prepared by dissolving 0.1 mole (16.19 g) of $MnCl_2.2H_2O$ in 500 ml solution using a volumetric flask. 10 ml of this solution is taken in a beaker and 5 ml concentrated HCl is added. The resulting solution is diluted to 125 ml. After this the solution is almost neutralize with diluted ammonia solution. In this solution, 20 g of NH_4Cl and 2 g of $(NH_4)_2HPO_4$ are added. The solution is heated to 90-95 ^{0}C and diluted ammonia solution is added drop wise with constant stirring. Due to this a precipitate of $Mn_3(PO_4)_2$ is formed. This solution is kept at room temperature for 3 hours. The precipitate is washed several times with distilled water and filtered on ash less filter paper. The precipitate along with the filter paper is put inside a pre weighted alumina crucible and heated at about 750 ^{0}C. The resulting material is weighted as $Mn_2P_2O_7$ to constant weight.

Reactions involving in this procedure are as follows.

$$Mn^{2+} + 2NH_3 + 2H_2O \rightarrow Mn(OH)_2 + 2NH_4^+$$

$$Mn^{2+} + NH_3 + HPO_4^{2-} \rightarrow Mn(NH_4)PO_4 \downarrow$$

$$3Mn^{2+} + 2HPO_4^{2-} \rightarrow Mn_3(PO_4)_2 + 2H^+ \downarrow$$

Procedure followed in Sections 3.1.1 and 3.1.2 is taken from References 25 and 29.

3.1.3 Synthesis of $MnFe_2O_4$ nanoparticles

Two different samples of $MnFe_2O_4$ are synthesized by coprecipitation method [24, 25]. For this NaOH solution is added drop wise in solutions containing Mn^{2+} and Fe^{3+} ions, in appropriate ratio, with constant stirring until pH of the system reaches to 10 and 12. The chemical reaction undergoing in this process is as follows.

$$Mn^{2+} + 2\ Fe^{3+} + x\ OH^- \rightarrow MnFe_2O_4 + (x\text{-}8)\ OH^- + 4\ H_2O$$

In a 250 ml beaker solutions of $FeCl_3$ and $MnCl_2$ are taken such that ratio of Mn^{2+} and Fe^{3+} ions is 1:2. In this solution 2 M NaOH solution is added drop wise at room temperature with constant stirring until pH of the system reaches to 10. The precipitate formed is washed many times with distilled water and dried at 60 ^{0}C. Finally the dried sample is grinded. The X-ray diffraction pattern of the powder thus prepared is shown in Figure 3.1. From this pattern it is clear that the prepared powder sample of $MnFe_2O_4$ is amorphous.

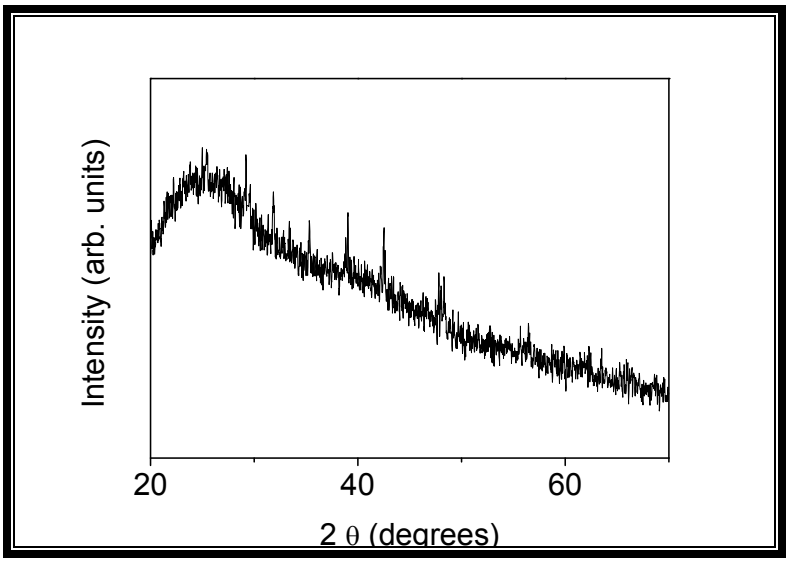

Figure 3.1: Room temperature X-ray diffraction pattern of amorphous $MnFe_2O_4$.

In a 250 ml beaker prepared solutions of $FeCl_3$ and $MnCl_2$ are taken keeping the ratio of Mn^{2+} and Fe^{3+} ions to be 1:2. In this 2 M NaOH solution is added drop wise with constant stirring and maintaining the temperature of the solution at 95 ^{0}C, until the pH of the system reached to 10. The resulting precipitate is kept at 95 ^{0}C for 40 minutes and then allowed to cool. The precipitate is washed many times with distilled water and then dried at 60 ^{0}C for several hours. The material is grinded for further use. The room temperature X-ray diffraction pattern of the synthesized powder sample is shown in figure 3.2(a). It is clear that the powder sample is single phase $MnFe_2O_4$.

I also prepare one more sample of $MnFe_2O_4$ nanoparticles by following same procedure at pH 12. The room temperature X-ray diffraction pattern of this sample is shown in Figure 3.2(b).

3.2 Structural Characterization

Figure 3.2(a) shows room temperature X-ray diffraction pattern of the $MnFe_2O_4$ sample synthesized at pH 10. This figure shows that the peaks are broadened. This is due to the nanocrystalline nature of the sample. The average crystallite (t) size is calculated using the modified Scherrer formula

$t = 0.9 \lambda / Cos\ \theta_B (b_m - b_s)$

where λ is the wavelength of the X-ray used, θ_B is the Bragg angle, b_m is the full width at half-maximum (FWHM) of a peak in radians and b_s is the FWHM of the same peak of a standard sample. The most intense peak in the Figure 3.2(a) is used to calculate the average crystalline size. This turns out to be about 7 nm. The use of $(b_m - b_s)$ instead of b_m in the Scherrer formula takes care of instrumental broadening.

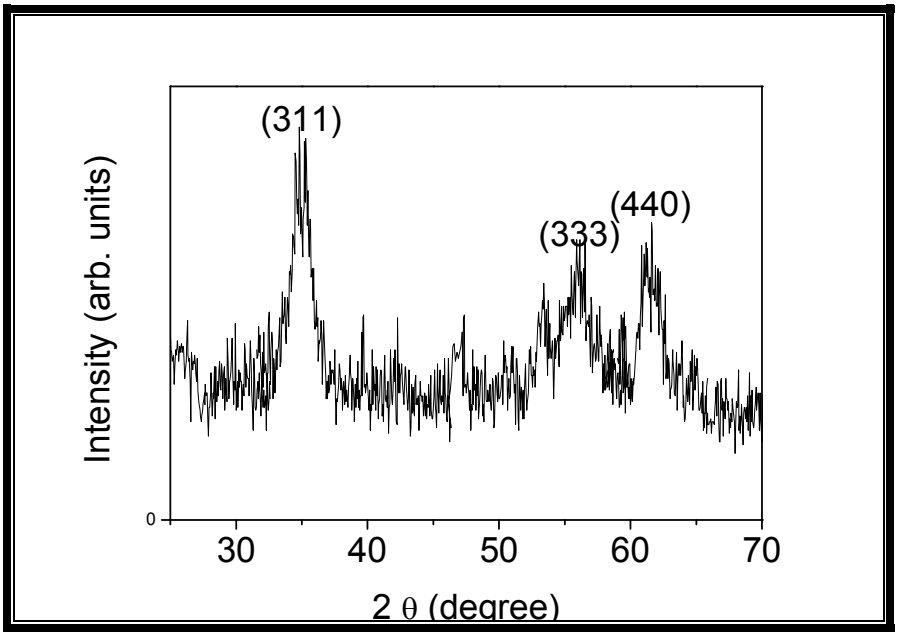

Figure 3.2(a): Room temperature X-ray diffraction pattern of $MnFe_2O_4$ nanoparticles synthesized at pH 10. Lower intensity peaks are not visible.

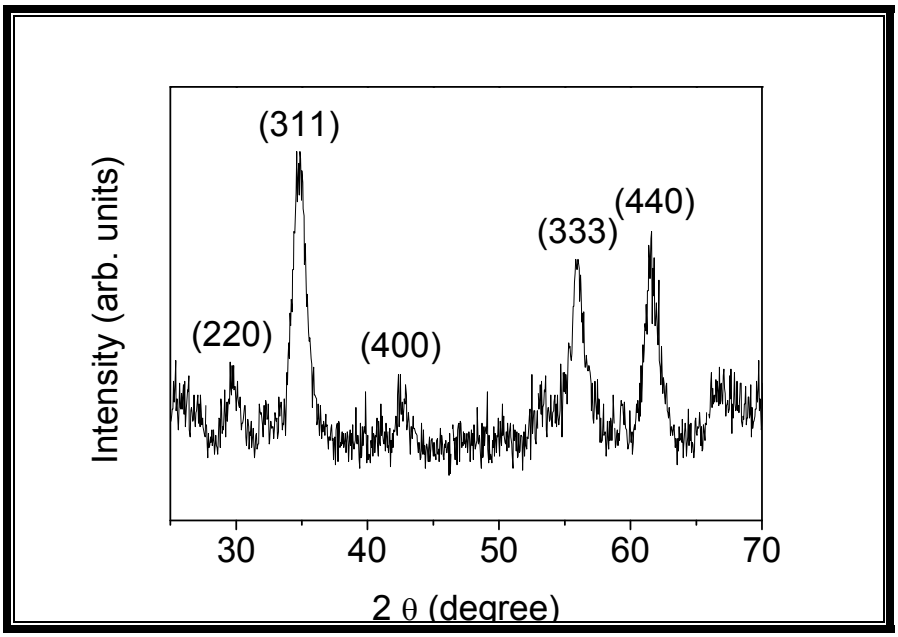

Figure 3.2(b): Room temperature X-ray diffraction pattern of $MnFe_2O_4$ nanoparticles synthesized at pH 12.

Figure 3.2(b) shows room temperature X-ray diffraction patterm of the sample synthesised at pH 12. The average crystallite size of this sample is also calculated using the modified Scherrer formula. It turns out to be about 9 nm.

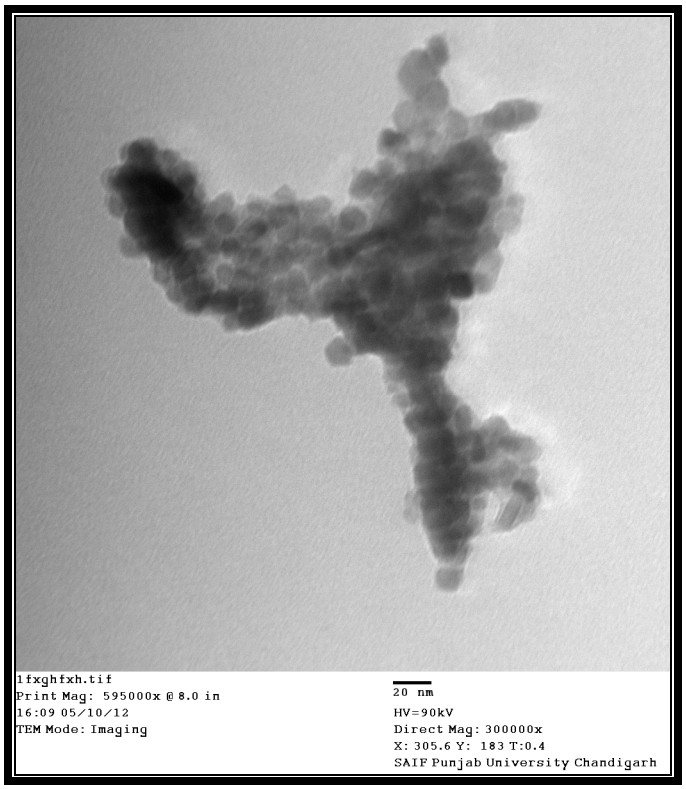

Figure 3.3(a): Transmission electron micrograph of $MnFe_2O_4$ nanoparticles synthesized at pH 10.

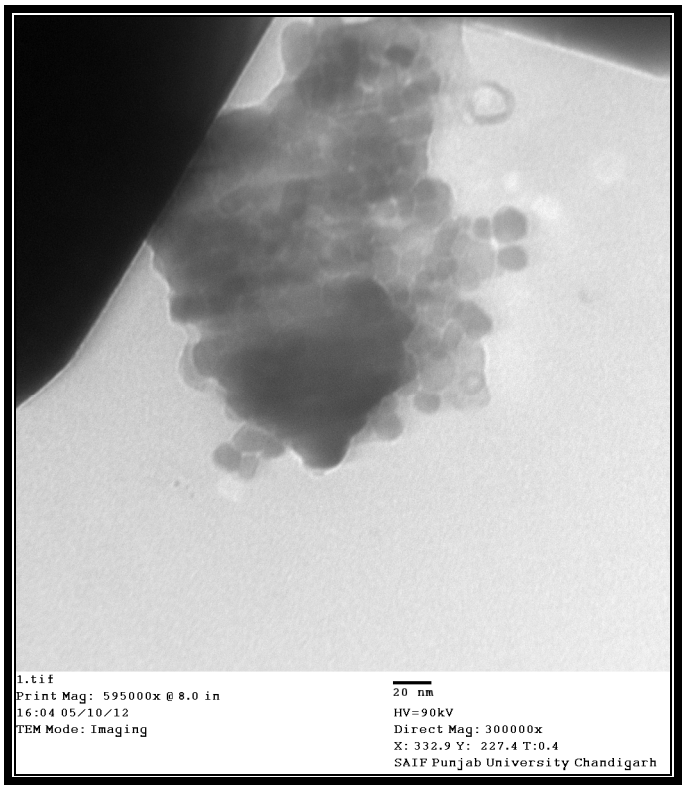

Figure 3.3(b): Transmission electron micrograph of $MnFe_2O_4$ nanoparticles synthesized at pH 12.

Both of the synthesised samples are also characterized by transmission electron microscope. For this the powder samples are dispersed in methyl alcohol and a drop of these dispersions are allowed to dry on the transmission electron microscopy grids. The micrographs thus obtained are shown in Figures 3.3(a) and 3.3(b). From these micrographs it is clear that the particles are on average about 7 and 9 nm respectively.

3.3 Magnetization Measurements

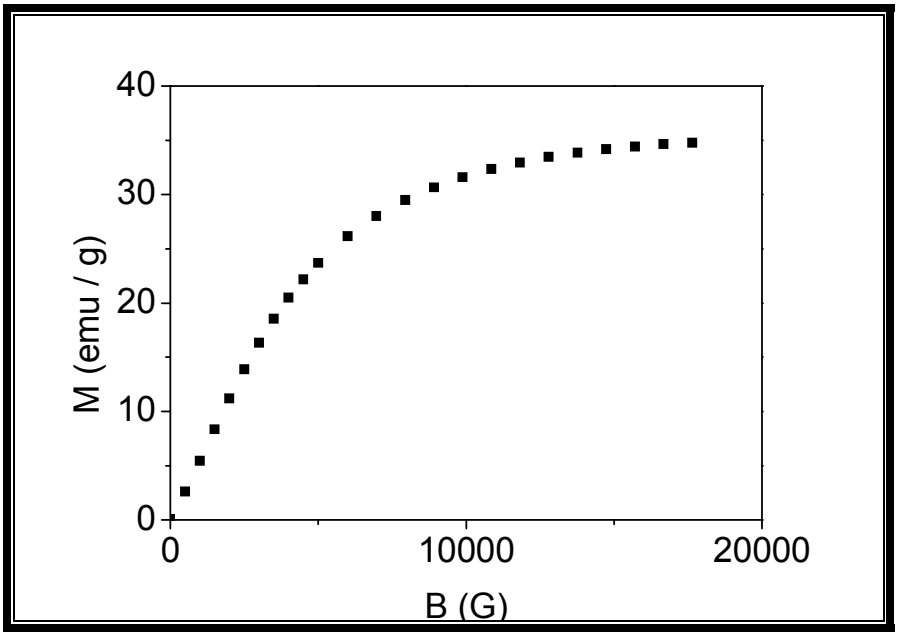

Figure 3.4(a): Magnetization *M* as a function of applied magnetic field *B* for 7 nm $MnFe_2O_4$ particles at room temperature.

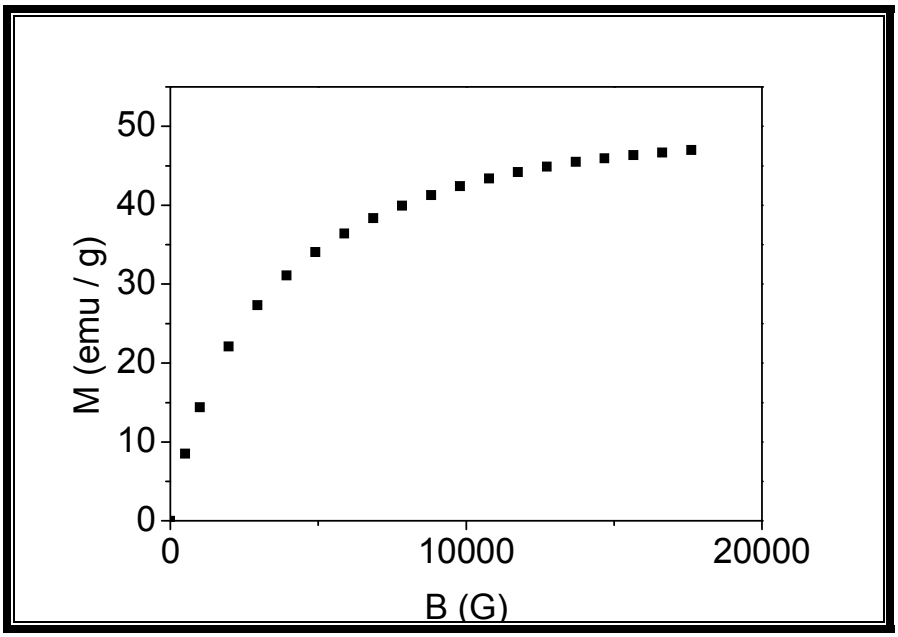

Figure 3.4(b): Magnetization *M* as a function of applied magnetic field *B* for 9 nm $MnFe_2O_4$ particles at room temperature.

Magnetic properties of the synthesized samples of $MnFe_2O_4$ nanoparticles are studied with the help of vibrating sample magnetometer. For this 15 mg of powder samples are packed inside Teflon tape for the magnetization measurements. Figure 3.4(a) shows magnetization *M* vs. applied magnetic field *B* for 7 nm $MnFe_2O_4$ particles at room temperature. This figure shows that the magnetization increases with increasing magnetic field and saturates at higher magnetic fields. In higher magnetic fields all the particle magnetic moments align themselves along the applied field direction giving rise to saturation of the magnetization.

Figure 3.4(b) shows magnetization *M* vs. applied magnetic field *B* for 9 nm $MnFe_2O_4$ particles at room temperature. This figure also shows that the magnetization increases

with increasing magnetic field and saturates at higher magnetic fields. In high magnetic fields all the particle magnetic moments align themselves along the applied field direction giving rise to saturation of the magnetization.

From figures 3.4(a) and 3.4(b) it is noted that the saturation magnetization of $MnFe_2O_4$ nanoparticles decreases with decreasing particle sizes. The fraction of atoms lying on the surface of the particle increases with decreasing particle size. Also the surface atoms suffer from different disorders. Because of these reasons the saturation magnetization of $MnFe_2O_4$ nanoparticles decreases with decreasing particle size.

Magnetizations of the samples are also measured as a function of temperature using the vibrating sample magnetometer to determine its Curie temperature T_C. For this 18 mg of the powder sample is packed inside aluminum foil. The Magnetization as a function of temperature in applied magnetic field of 1000 G is shown in Figures 3.5(a) and 3.5(b) for the 7 and 9 nm samples respectively.

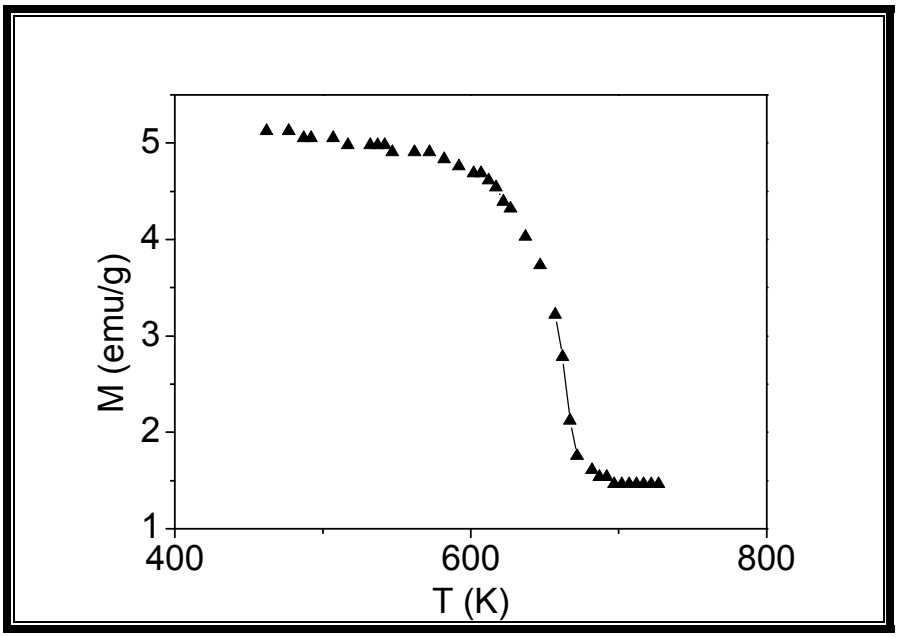

Figure 3.5(a): Magnetization as a function of temperature for 7 nm $MnFe_2O_4$ nanoparticles in 1000 G applied magnetic field.

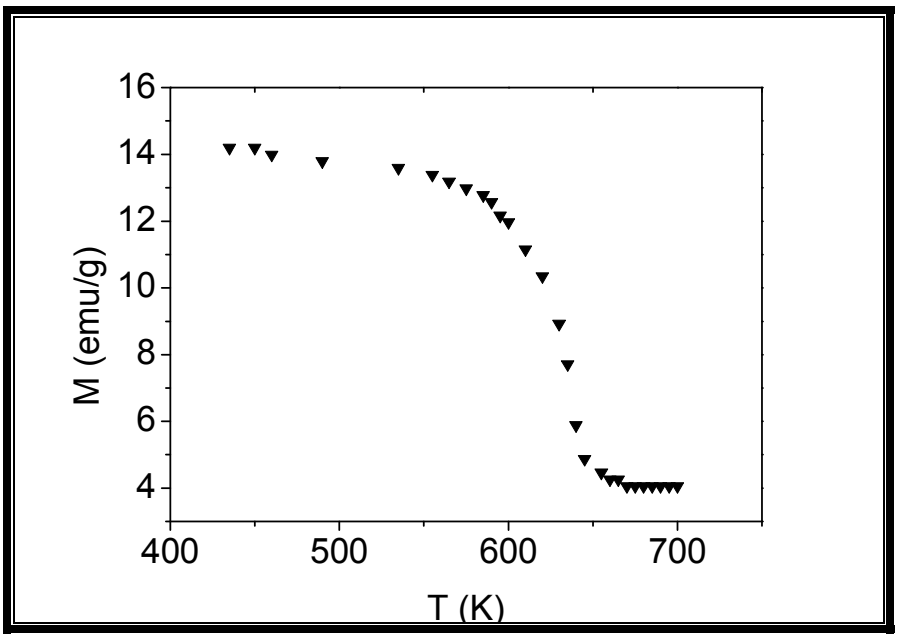

Figure 3.5(b): Magnetization as a function of temperature for 9 nm $MnFe_2O_4$ nanoparticles in 1000 G applied magnetic field.

From Figure 3.5(a) it is observed that the magnetization decreases slowly with increasing temperature initially and then the same suddenly starts decreasing with increasing temperature drastically up to 695 K. The magnetization of the system does not change significantly for any further increase in the temperature. This measurement indicates that the Curie temperature T_C of the 7 nm $MnFe_2O_4$ nanoparticles is about 695 K. The magnetization of 9 nm $MnFe_2O_4$ nanoparticles also varies in similar manner. It is shown in Figure 3.5(b). From this figure the Curie temperature of 9 nm $MnFe_2O_4$ nanoparticles is found to be about 655 K. Value of Curie temperatures for both the samples are larger than the Curie temperature of bulk $MnFe_2O_4$.

Chapter 4

Conclusions

In this work two samples of $MnFe_2O_4$ nanoparticles are synthesized with the help of coprecipitation method using $MnCl_2$ and $FeCl_3$ aqueous solutions. This method results in the formation of pure $MnFe_2O_4$ nanoparticles. The average crystallite sizes are found to be about 7 and 9 nm using the modified Scherrer formula. The average particle sizes are also confirmed from the transmission electron micrographs. The room temperature magnetization as a function of applied magnetic field measurements indicate for the superparamagnetic nature of the samples. The Curie temperature of the both samples are found to be larger than the Curie temperature of the bulk sample.

In this work two samples of $MnFe_2O_4$ nanoparticles are synthesized. In future one may synthesize monodispersed samples of $MnFe_2O_4$ nanoparticles of different sizes and may study their size dependent magnetic properties.

References

[1] V. Raghavan, *Materials Science and Engineering* (PHI Learning Private Limited, Fifth Edition, 2010).

[2] C. Kittel, *Introduction to Solid State Physics* (John Wiley and Sons, Inc., Seventh Edition, 1996).

[3] W. F. Smith and J. Hashemi, *Foundation of Materials Science and Engineering* (McGraw Hill International Edition, Fourth Edition, 2006).

[4] S.O. Pillai, *Solid State Physics* (New Age Techno Press, 6th ed., 2010).

[5] http://www.vectorsite.net/tpqm_04.html

[6] www.irm.umn.edu/hg2m/hg2m_b/hg2m_b.html

[7] http://www.ndt-ed.org/EducationResources/CommunityCollege/MagParticle/Physics/HysteresisLoop.htm

[8] http://accessscience.com/content/Curie%20temperature/173700

[9] http://www.tf.unikiel.de/matwis/amat/elmat_en/kap_4/backbone/r4_1_3.htm

[10] http://www.tuchemnitz.de/physik/OFGF/research/magnetic_recording.php

[11] http://wikis.lib.ncsu.edu/index.php/Spinel

[12] F. S. James and K M. Madanapalli, *Introduction to Materials Science for Engineers* (Pearson Education, 6th ed., 2005).

[13] B. D. Cullity and C. D. Graham, *Introduction to Magnetic Materials* (John Wiley and Sons, 2nd ed., 2009).

[14] D. R. Askeland and P.P. Phulé, *The Science and Engineering of Materials* (4th ed., 2004).

[15] http://www.scribd.com/doc/55725280/11/Stress-Anisotropy

[16] B. D. Cullity and C. D. Graham , Introduction to Magnetic Materials (John Wiley and Sons , 2nd ed.,2009).

[17] Susan Sam and ,A. Samson Nesaraj; International Journal of Applied Science and Engineering **9**, 223 (2011).

[18] N.S. Gajbhiye and G. Balaji , Thermochimica Acta **385**; 143 (2002).

[19] J. Amighian, M. Nozaffer and B. Nasr, Physica Status Solidi C, Current Topics in Solid State Physics **3**, 3188 (2006).

[20] M. A. Ahmed, N. Okasha and S I El-Dek. Nanotechnology **19** (2008) 065603.

[21] T. V. Solis, P. V. Vigon, S. Alvarez, G. Marban and A. B. Fuertes, Catalysis Communication **8**, 2037 (2007).

[22] N. M. Deraz and S. Shaban, Journal Analytical and Applied Pyrolysis **86**, 173 (2009).

[23] Aria Yang, C N Chinnasamy, J M Greneche, Yajie Chen, Soack D Yoon, Zhaohui Chen, Kailin Hsu, Zhuhua Cai, Kate Ziemer, C Vittoria and V G Harris, Nanotechnology **20** 185704 (2009).

[24] R. V. Upadhyay, K. Parekh, and R. V. Mehta, Phys. Rev. B **68**, 224434 (2003).

[25] Synthesis and characterization of manganese ferrite nanoparticles, M. Tech. thesis by Romi Bharol (2011).

[26] http://tap.iop.org/atoms/xray/530/page_47297.html

[27] http://www.hk-phy.org/atomic_world/tem/tem02_e.html

[28] http://www.el.utwente.nl/tdm/istg/research/vsm/vsm.htm

[29] Vogel's textbook of quantitative chemical analysis (5^{th} ed.; revised by G. H. Jeffery et al., Longman Scientific and Technical, 1989).